The histone H3.3K36M mutation reprograms the epigenome of chondroblastomas

Dong Fang[1*], Haiyun Gan[1*], Jeong-Heon Lee[1,2*], Jing Han[1*], Zhiquan Wang[1*], Scott M. Riester[3], Long Jin[3], , Jianji Chen[4], Hui Zhou[1], Jinglong Wang[5,6], Honglian Zhang[1], Na Yang[5], Elizabeth W. Bradley[3], Thai Ho[7], Brian P. Rubin[8], Julia A. Bridge[9], Stephen N Thibodeau[10], Tamas Ordog[2,11,12], Yue Chen[4], Andre J. van Wijnen[1,3], Andre M. Oliveira[3,10], Rui-Ming Xu[5,6], Jennifer J. Westendorf[1,3], Zhiguo Zhang[1,2,13]

[1]Department of Biochemistry and Molecular Biology, Mayo Clinic College of Medicine, 200 First St SW, Rochester, MN 55905

[2]Epigenomic Translation Program, Center of Individualized Medicine, Mayo Clinic College of Medicine, 200 First St SW, Rochester, MN 55905

[11]Department of Physiology and Biomedical Engineering, Division of Gastroenterology and Hepatology, Mayo Clinic College of Medicine, 200 First St SW, Rochester, MN 55905
[12] Interdisciplinary Health Science Initiative, 1110 Micro & Nanotechnology Lab, M/C 249, University of Illinois Urbana-Champaign, Urbana, IL 61801 (Research Affiliate)

[3]Department of Orthopedic Surgery, Mayo Clinic College of Medicine, 200 First St SW

Rochester, MN 55905

[4]Department of Biochemistry, Molecular Biology and Biophysics, University of Minnesota at Twin Cities, Minneapolis, MN 55455

[5]National Laboratory of Biomacromolecules, Institute of Biophysics, Chinese Academy of Sciences, 5 Datun Road, Beijing, 100101, [6]University of Chinese Academy of Sciences, 19A Yuquan Road, Beijing 100049.

[7]Division of Hematology/Oncology, Mayo Clinic Arizona, 13400 East Shea Blvd

Scottsdale, AZ 85259

[8] Robert J. Tomsich Department of Pathology and Laboratory Medicine Institute and Department of Cancer Biology, Cleveland Clinic and Lerner Research Institute, L2 9500 Euclid Avenue Cleveland, OH 44195

[9]Department of Pediatrics and Orthopedic Surgery 983135 Nebraska Medical Center Omaha, NE 68198-3135

[10]Department of Laboratory Medicine and Pathology, Mayo Clinic College of Medicine, 200 First St SW, Rochester, MN 55905

These authors contributed equally to this work

[13]Corresponding Author:

zhang.zhiguo@mayo.edu

Phone: 507-538-6074; Fax: 507-284-9759

Running Title: H3.3K36 mutation and the cancer epigenome

Supplemental Figures

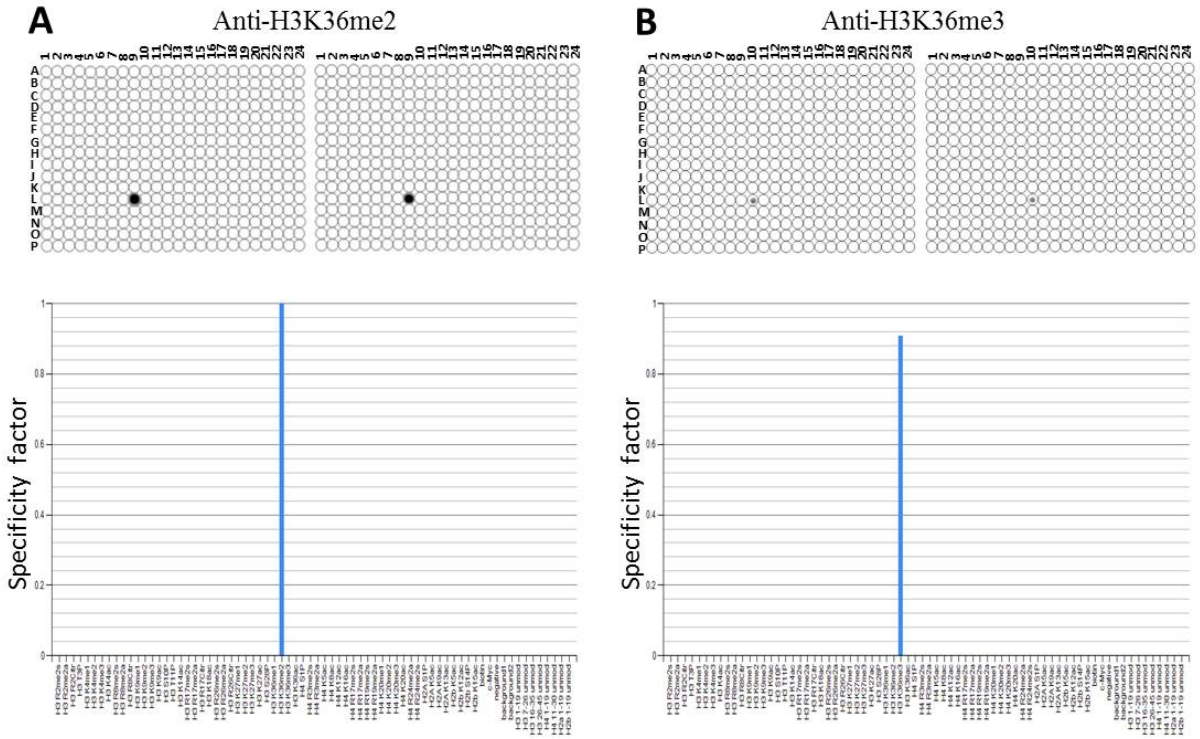

Figure S1. The anti-H3K36me2 and anti-H3K36me3 antibodies are specific for their targets. (**A**) Antibodies against H3K36me2 are specific. The MODified™ Histone Peptide Array (Active Motif, Cat.# 13005, lot # 32412003) was probed with antibodies against H3K36me2 (Cell Signaling Technology, Cat.# 2901, lot 5) and was visualized by a chemiluminescent detection system according to the manufacturer's instructions. The arrays were scanned with Array Analysis Software 7 (top) and the results were plotted. Active Motif's Array Analyze Software was used to analyze spot intensity. The results were shown as a specificity factor, which is the ratio of the average intensity of all spots containing the mark divided by the average intensity of all spots not containing the mark (bottom). (**B**) Antibodies against H3K36me3 are specific. The MODified™ Histone Peptide Array was probed with antibodies against H3K36me3 (Active Motif, cat. # 61101, lot 32412003) and analyzed as described in (A).

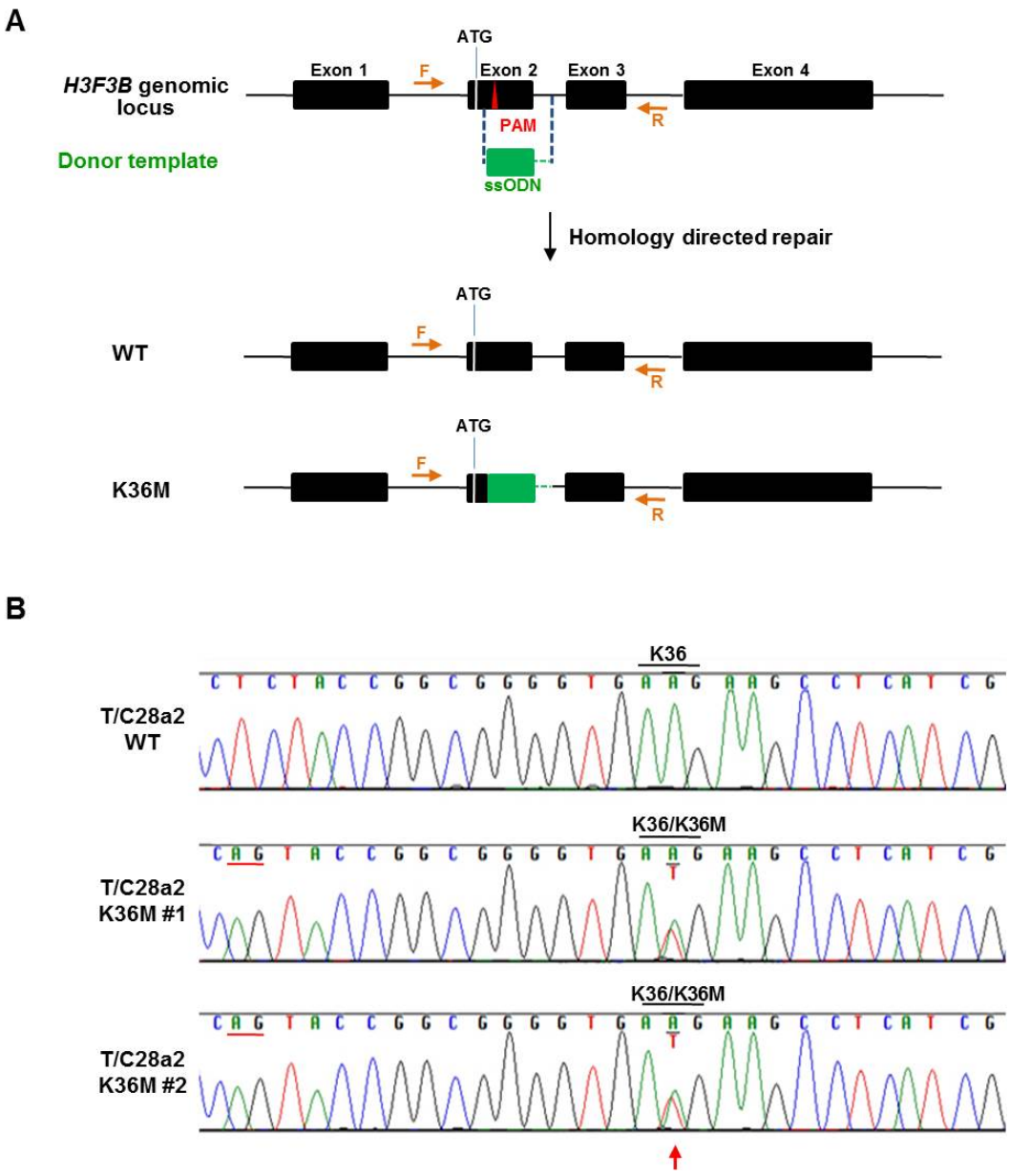

Figure S2. (**A**) Generation of genomic H3.3K36M knock-in mutation in the *H3F3B* locus via CRISPR/Cas9 genome editing. The locations of the H3.3K36 target site and sequencing primers were shown in the 5.5 kb region of human *H3F3B* gene locus in chromosome 17. A primer pair (F and R) was designed outside of the homology arms of the single-stranded oligodeoxynucleotide (ssODN). ATG indicates the translation start codon of histone H3.3. PAM: Protospacer adjacent motif. (**B**) Sanger sequencing confirms one allele of the *H3F3B* gene is mutated in two independent cell lines. Genomic DNA was isolated from each clone and subjected to PCR using the primer pair surrounding the target site. The resulting PCR products (690 bp) were sequenced to determine the genotype in the *H3F3B* locus. The arrow indicates the location of the knock-in mutation site. The presence of A/T nucleotides in two T/C 28a2 cell lines indicates the mutation at one allele of *H3F3B* gene in both clones.

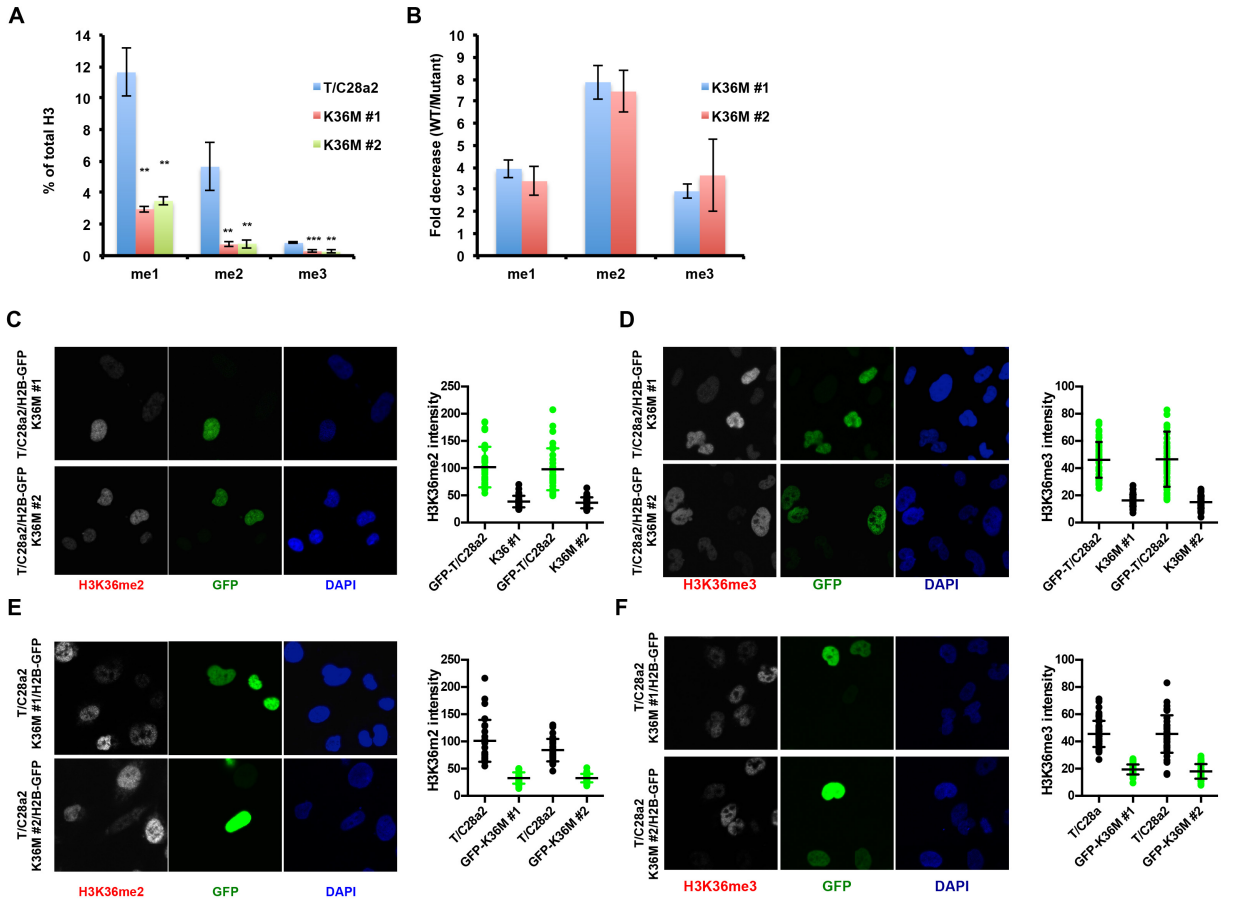

Figure S3. The H3K36 methylation levels are reduced in two H3.3K36M mutant chondrocyte lines. (**A**) Histone proteins were isolated from T/C28a2 cells and two H3.3K36M mutant lines using acid extraction and subjected to quantitative mass-spectrometry analysis of mono-, di-, and tri-methylated H3K36 (H3K36me1, me2, and me3). Results (mean ± SD, **P<0.01, ***P<0.001) from three independent experiments were shown. (**B**) Normalized fold of reduction of H3K36me1, H3K36me2 and H3K36me3 in two H3.3K36M mutant lines compared to control T/C28a2 cells by mass-spectrometry analysis. (**C-D**) Analysis of H3K36me2 and H3K36me3 levels by immunofluorescence (IF). T/C28a2 (WT) cells were transduced with lenti-virus expressing H2B-GFP. The GFP-marked cells were then mixed with uninfected H3.3K36M cells for IF using antibodies against H3K36me2 (C) and H3K36me3 (D). Right panels show the quantification of the H3K36me2 or H3K36me3 fluorescence intensity. At least 50 GFP positive or negative cells were measured from each experiment. (**E-F**) The experiments were performed as described above except that H3.3K36M mutant cells were marked with GFP before mixing with T/C28a2 cells for IF. The experiments from C-F were repeated twice and similar results were obtained. Results from one representative experiment are shown.

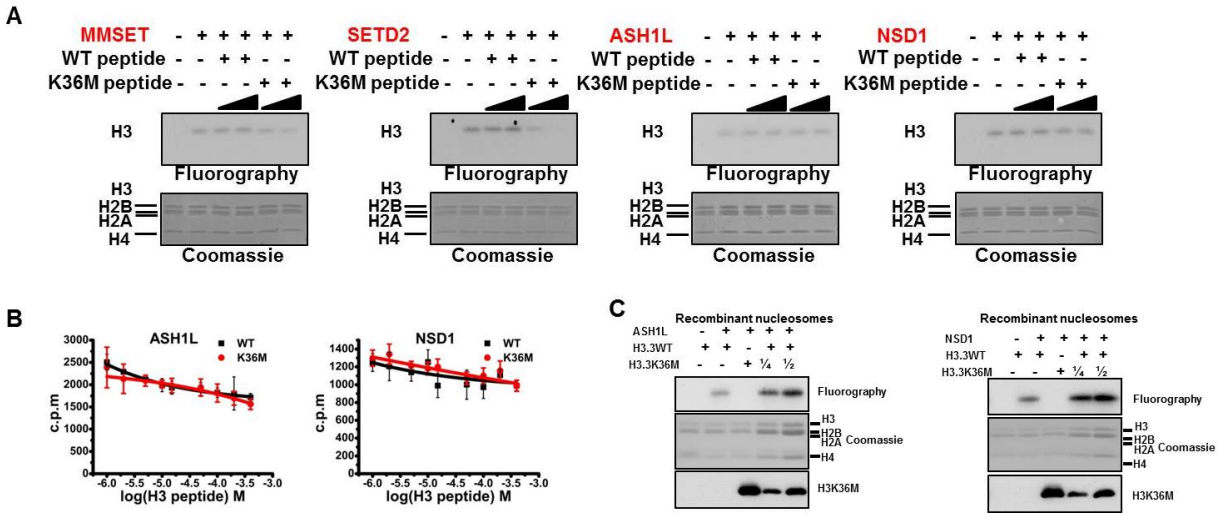

Figure S4. H3.3K36M selectively inhibits the enzymatic activity of MMSET and SETD2. (**A**) H3.3K36M peptide selectively inhibits the enzymatic activity of MMSET and SETD2. Histone methyltransferase assays were performed as described in Fig. 1C. Reaction mixtures were resolved by 15% SDS-PAGE and examined by Coomassie blue staining (lower panel) or fluorography (upper panel). (**B**) H3.3K36M peptides do not inhibit the enzymatic activity of ASH1L or NSD1. Histone methyltransferase assays were performed as described in Fig. 1C. (**C**) The H3.3K36M-containing mononucleosomes do not inhibit the enzymatic activities of ASH1L or NSD1 *in vitro*. The HMT assays were performed as described in Fig. 1D and methylated H3 was detected by fluorography. H3.3K36M mutant proteins were detected by H3K36M antibodies.

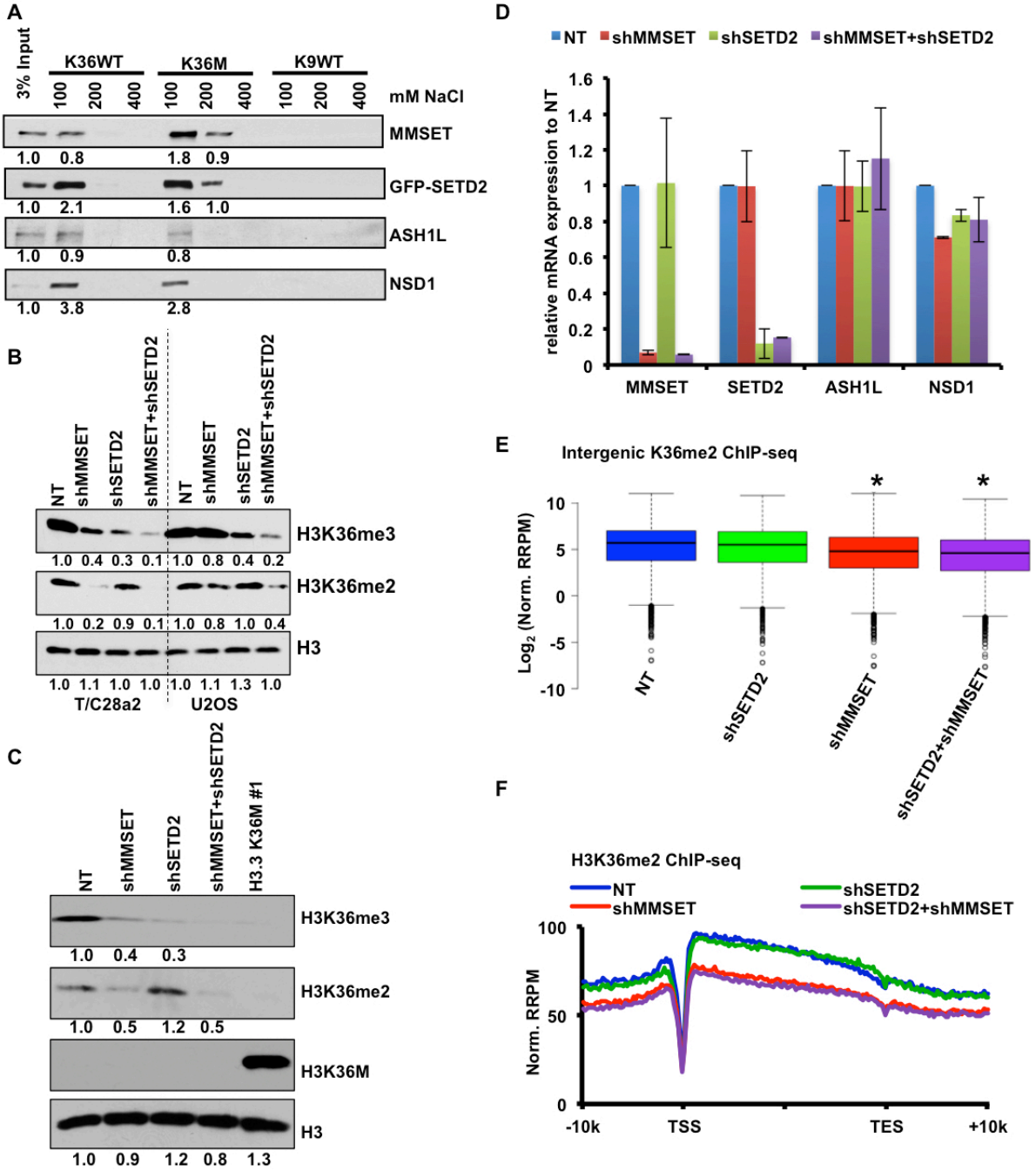

Figure S5. Effect of MMSET and SETD2 depletion on H3K36me2 and H3K36me3 in T/C28a2 and U2OS cells. (**A**) More MMSET and SETD2 bind to the H3.3K36M peptide than corresponding H3.3 peptide. H3.3K36M peptide and its corresponding H3.3 peptide as well as a H3K9 peptide was cross-linked to beads and used to pull down proteins from cell extracts prepared from 293T cells expressing GFP-SETD2. Beads were washed with different salt concentrations. Proteins in input and pull-down were analyzed by Western blot. The intensity of each blot was quantified by ImageJ (bottom of each Western blot), with the blot of input set to 1. (**B**) Depletion of MMSET, but not SETD2, leads to a reduction in H3K36me2 in both T/C28a2 and U2OS cells. Depletion of MMSET affects H3K36me3 only in T/C28a2

cells, but not in U2OS cells. The later results are consistent with published data (*11*). SETD2 depletion reduces H3K36me3 in both T/C28a2 and U2OS cells. Histones were isolated using acid extraction from non-targeted (NT) control cells or cells depleted of MMSET, SETD2 or both, and were analyzed by Western blot. (**C**) T/C28a2 cells with MMSET depletion have a higher level of H3K36me2 than cells expressing H3.3K36M mutant proteins. Histones were isolated from non-targeted (NT) control cells, cells depleted of MMSET, SETD2 or both, or one H3.3K36M clone, and were analyzed by Western blot. The intensity of each Western blot analysis in B and C was quantified as described above, with the intensity of each blot in NT control cells set to 1. (**D**) Depletion of MMSET or SETD2 in T/C28a2 cells does not affect expression of other methyltransferases (ASH1L, NSD1, MMSET and SETD2). The expression of MMSET, SETD2, ASH1L and NSD1 was analyzed in cells treated as in (B) by RT-PCR and normalized to results from the NT control. (**E-F**) Normalized tag distribution profiles of H3K36me2 for intergenic regions (E) and gene bodies (F) in non-targeted (NT) control cells, cells depleted with MMSET, SETD2 alone or in combination. RRPM: reference-adjusted reads per million. P values were calculated by two-tailed Student's t test (* p value < 0.01). There are two non-exclusive explanations for the differential effect of H3.3K36M and MMSET depletion on H3K36me2 levels. First, in addition to MMSET, a yet-to-be-identified H3K36 methyltransferase may be inhibited by H3.3K36M mutant proteins. Second, it is possible that MMSET is the predominant H3K36me2 methyltransferase inhibited by H3.3K36M mutant proteins. But MMSET depletion by shRNA is not sufficient low enough compared to inhibition by H3.3K27M mutant proteins. Alternatively, it may take cells longer than 72 hours (the time at which we analyzed the effect of MMSET depletion) to remove H3K36me2 *in vivo*.

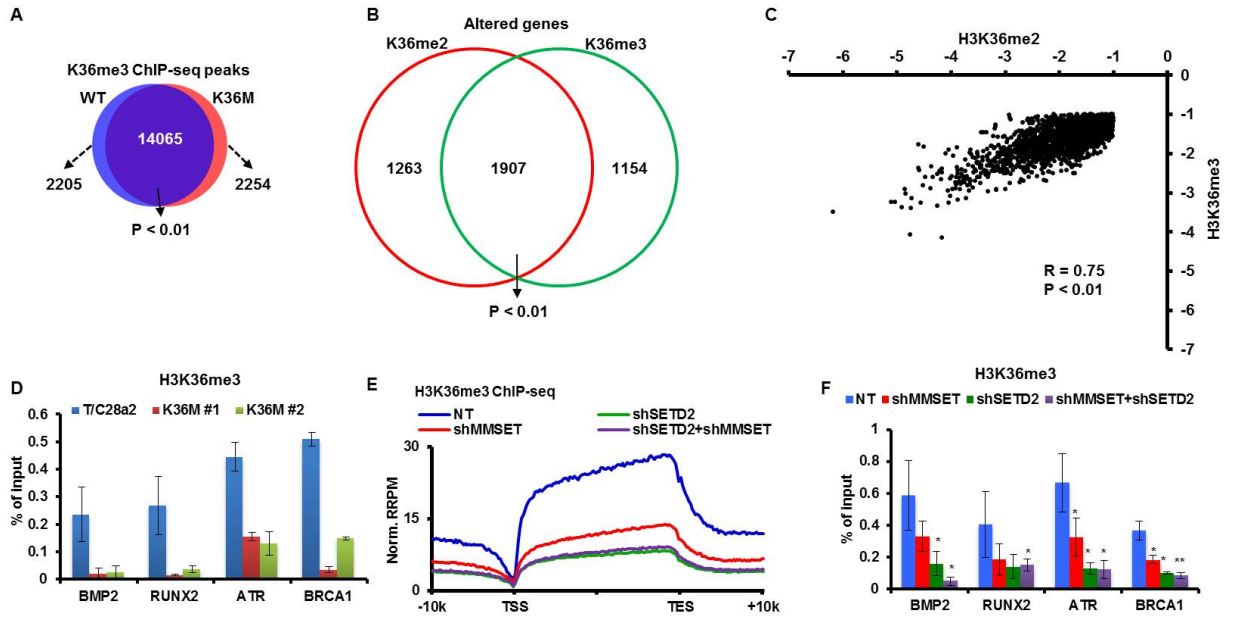

Figure S6. H3K36me2 and H3K36me3 are co-reduced at gene bodies. (A) Venn diagram of H3K36me3 peaks in WT and H3.3K36M T/C28a2 cells. (B) Venn diagram of the genes with altered H3K36me2 or H3K36me3 occupancies at gene bodies. Genes with altered H3K36me2 and H3K36me3 were chosen based on analysis of ChIP-seq read counts at gene bodies by DEseq (*22*) with a cutoff p value of 10^{-5}. The p value for the Venn diagram in A and B was calculated by the hypergeometric test. (C) Genes with altered H3K36me2 levels at gene bodies correlate positively with the genes with altered H3K36me3. 1907 genes that show changes in both H3K36me2 and H3K36me3 in (B) were used to perform dot plot analysis. (D) Histone H3K36me3 is reduced at four gene loci in two H3K36M mutant cell lines compared to T/C28a2 cells. ChIP assays are performed using H3K36me3 antibodies and ChIP DNA was analyzed using real-time PCR amplifying gene bodies of indicated genes. Data represent the mean and deviations of two independent experiments. H3K36me3 levels at intergenic regions are very low and not analyzed. (E) The levels of H3K36me3 at gene bodies are reduced after depletion of MMSET, SETD2 alone or in combination. Reference-adjusted reads per million (RRPM) of H3K36me3 ChIP-seq were calculated from 10 Kb upstream of TSS to 10Kb downstream of TES sites. H3K36me3 ChIP-seq assays were performed after depletion of MMSET, SETD2 alone, or in combination (shMMSET+shSETD2) in T/C28a2 cells described Fig. S5D-F. (F) Depletion of SETD2 in T/C28a2 cells leads to reduction of H3K36me3 levels at indicated loci. Depletion of MMSET reduces H3K36me3 at two of four selected genes. H3K36me3 ChIP assays were performed after depletion of MMSET, SETD2 alone, or in combination (shMMSET+shSETD2) in T/C28a2 cells. ChIP DNA was analyzed by real-time PCR as described in the above. Results (mean ± SD, *P<0.05, **P<0.01) from three independent experiments were shown.

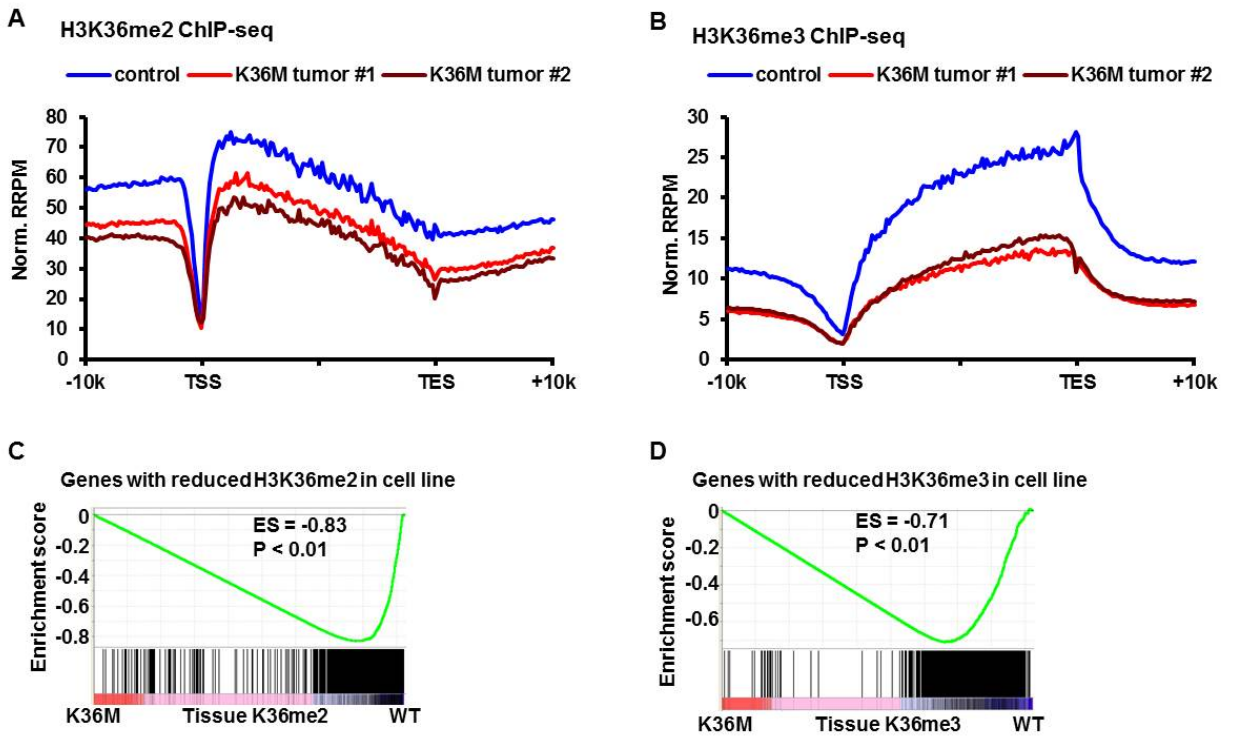

Figure S7. The levels of H3K36me2 (A) and H3K36me3 (B) at gene bodies are reduced in H3.3K36M chondroblastoma patient samples similarly to those in H3.3K36M mutant chondrocytes. H3K36me2 and H3K36me3 ChIP-seq were performed in two H3.3K36M positive chondroblastoma patient samples and normal human primary bone cells. To normalize ChIP efficiency, the same amount or ratio of yeast chromatin relative to the input chromatins was spiked into ChIP reactions. Reference-adjusted reads per million (RRPM) of H3K36me2 (A) or H3K36me3 ChIP-seq (B) were calculated from 10 Kb upstream of TSS to 10Kb downstream of TES sites. Please note that the fold of reduction of H3K36me2 in chondroblastoma samples was not as dramatic as in engineered H3.3K36M T/C282a cell lines likely due to cellular heterogeneity of chondroblastoma samples. (C-D) Gene set enrichment analysis (GSEA) was performed using genes with altered H3K36me2 (C) and H3K36me3 (D) occupancy at gene bodies. The enrichment plot is shown at the top. Black vertical lines indicate gene hits and the ranking metric scores based on the ratio of H3K36me2 ChIP-seq signals in patient tumor tissues. H3K36me2 and H3K36me3 ChIP-seq signals in human primary bone cells were used for normalization of the corresponding H3K36me2 and H3K36me3 ChIP-seq in chondroblastoma. ES, enrichment score.

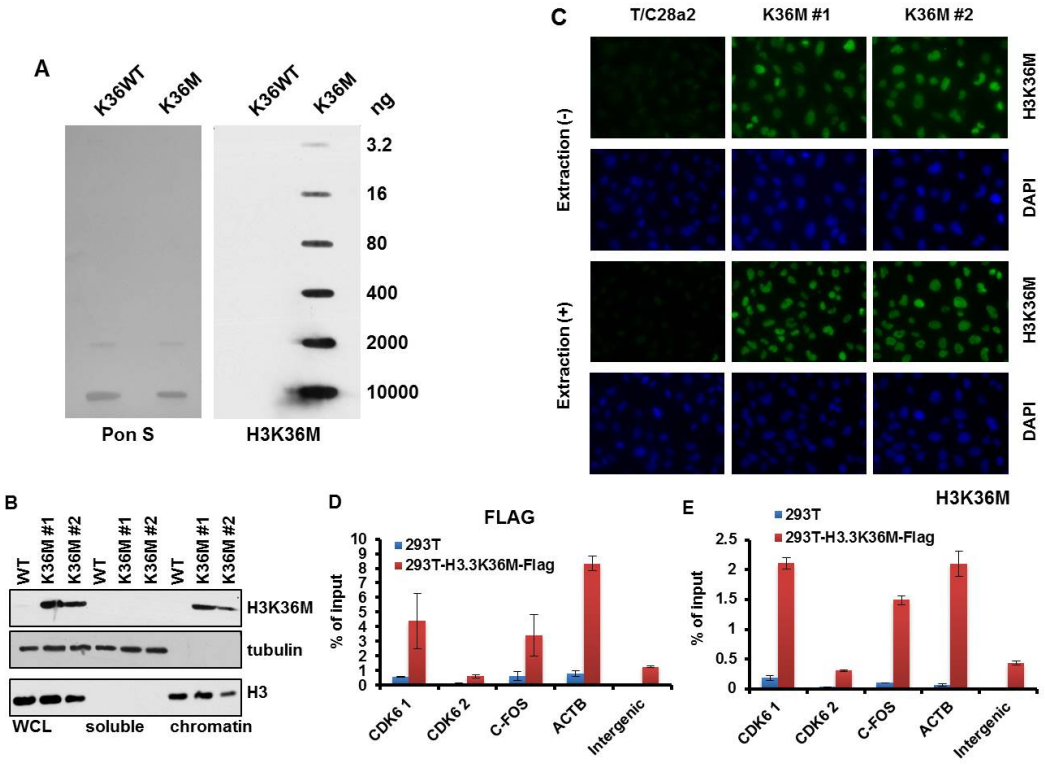

Figure S8. The H3K36M antibody specifically recognizes the H3.3K36M mutant protein and can be used for ChIP assays. (**A**) The H3K36M antibody specifically recognizes a H3K36M peptide *in vitro*. Left: Ponceau S staining of the membrane spotted with a H3.3 WT peptide and the corresponding H3.3K36M peptide. Right: Western blot analysis using the anti-H3K36M antibody. (**B**) The H3K36M protein is assembled into chromatin. Proteins were separated into soluble and chromatin bound fractions in T/C28a2 cell lines and detected by Western blot using indicated antibodies. (**C**) H3K36M mutant proteins bind to chromatin. Parental T/C28a2 and two H3.3K36M cells were fixed before (-) or after (+) being pre-extracted by Triton X-100. Cells were then used for immunofluorescence using the anti-H3K36M antibody. The nuclei were counterstained by DAPI. (**D-E**) The H3K36M antibody can be used for ChIP assays. ChIP assays were performed using the Anti-FLAG (D) or Anti-H3K36M (E) antibody in 293T cells with or without stable expression of H3.3K36M-FLAG proteins. ChIP DNA was analyzed using five different primer pairs targeting the genes indicated in figures and real-time PCR. Results represent the mean and standard deviations of two independent experiments. Please note that similar ChIP-PCR patterns at four genes and one intergenic region were observed for anti-FLAG antibodies and anti-H3.3K36M antibodies.

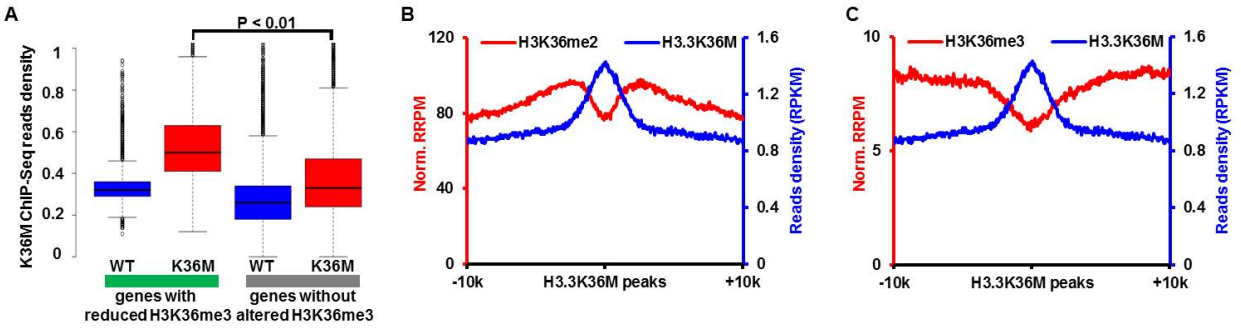

Figure S9. Inverse relationship between the H3K36M density and H3K36me2/me3 level. (**A**) H3K36M levels in genes with reduced H3K36me3 are significantly higher than those without altered H3K36me3. Genes were separated into two groups according to the changes of H3K36me3 levels in H3.3K36M cell lines compared to parental cells and H3.3K36M density was calculated at these two group of genes. P values were calculated by two-tailed Student's t test. (**B**) Inverse correlations between H3.3K36M and H3K36me2 ChIP-seq read densities. A 40-bp sliding window was used to scan 10Kb regions on both sides of H3.3K36M peak summits and overlapping H3K36me2 peaks. The red line represents the signal of H3K36me2 ChIP-seq using the RRPM as Y-scale, the blue line represents signal of H3.3K36M ChIP-seq using the traditional RPKM as Y-scale. The common H3.3K36M peaks from two H3.3K36M cell lines were used for the analysis and shown in Figure 3A. (**C**) H3K36me3 levels are low at H3K36M peaks. The red line represents the signal of H3K36me3 ChIP-seq using the RRPM as Y-scale and the blue line represents signal of H3K36M ChIP-seq using the traditional RPKM as Y-scale.

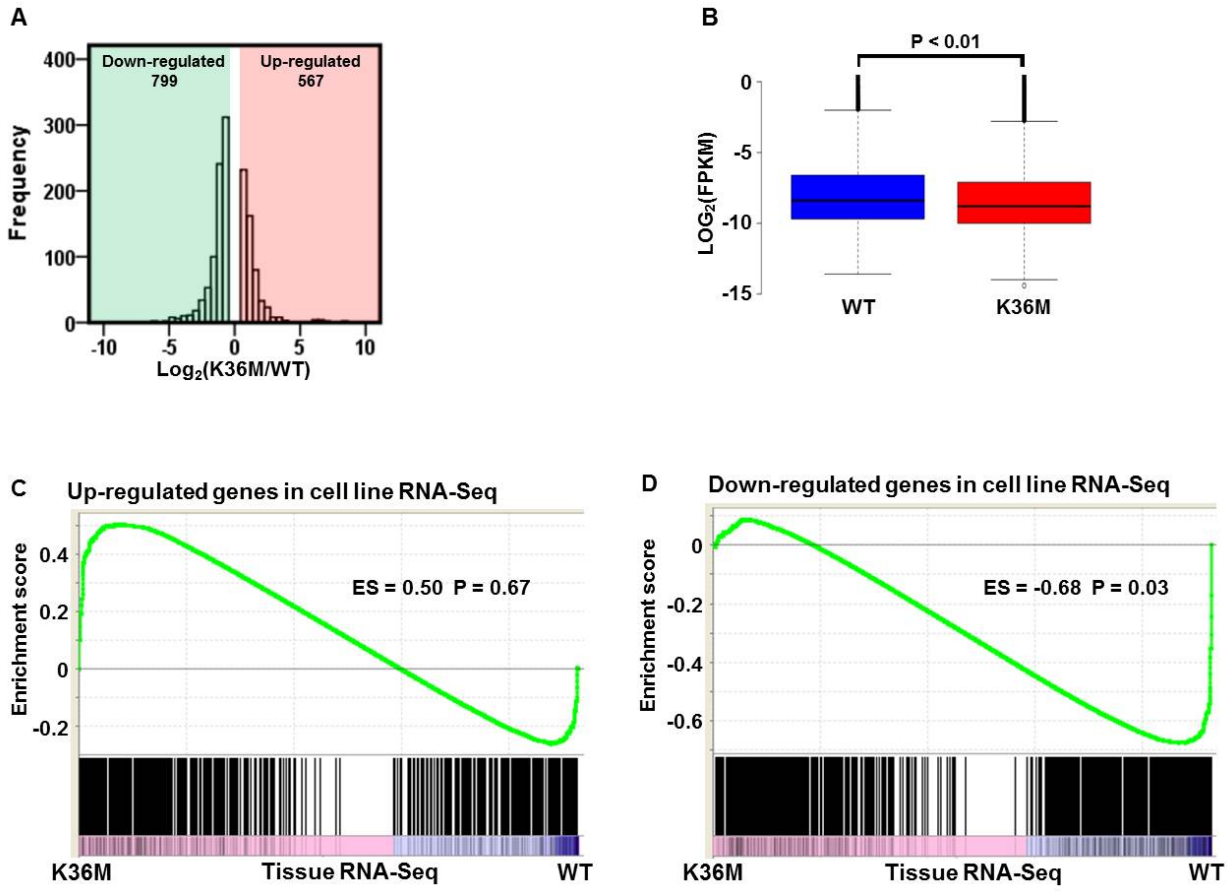

Figure S10. Effects of H3.3K36M on gene expression in H3.3K36M cell lines and tumors. (**A**) Histogram of differentially expressed genes in two H3.3K36M T/C28a2 cells compared to parental cells. RNA-seq was analyzed using Cufflink and the genes were selected based on FDR < 0.05. (**B**) The expression of intergenic regions in H3.3K36M mutant cells is lower than that wild type cells. Intergenic regions were defined based on ENCODE projects (http://www.gencodegenes.org/). Intergenic regions with significantly changed H3K36me2 (DEseq, p value < 10-5) were shown. FPKM for the intergenic regions were calculated from RNA-seq data. The p value was calculated using Student's t test. (**C**) Genes with increased expression in H3.3K36M cell lines were not enriched in genes with increased expression in tumor samples. (**D**) Genes with reduced expression in H3.3K36M cell lines were enriched in genes with reduced expression in chondroblastoma samples. Gene set enrichment analysis (*23*) plot of up- (C) and down-regulated (D) gene sets was obtained from cell lines. The enrichment plot is shown at the top. Black vertical lines indicate gene hits and the ranking metric scores based on the ratio of RNA-seq results in chondroblastomas and normal human primary chondrocyte cells.

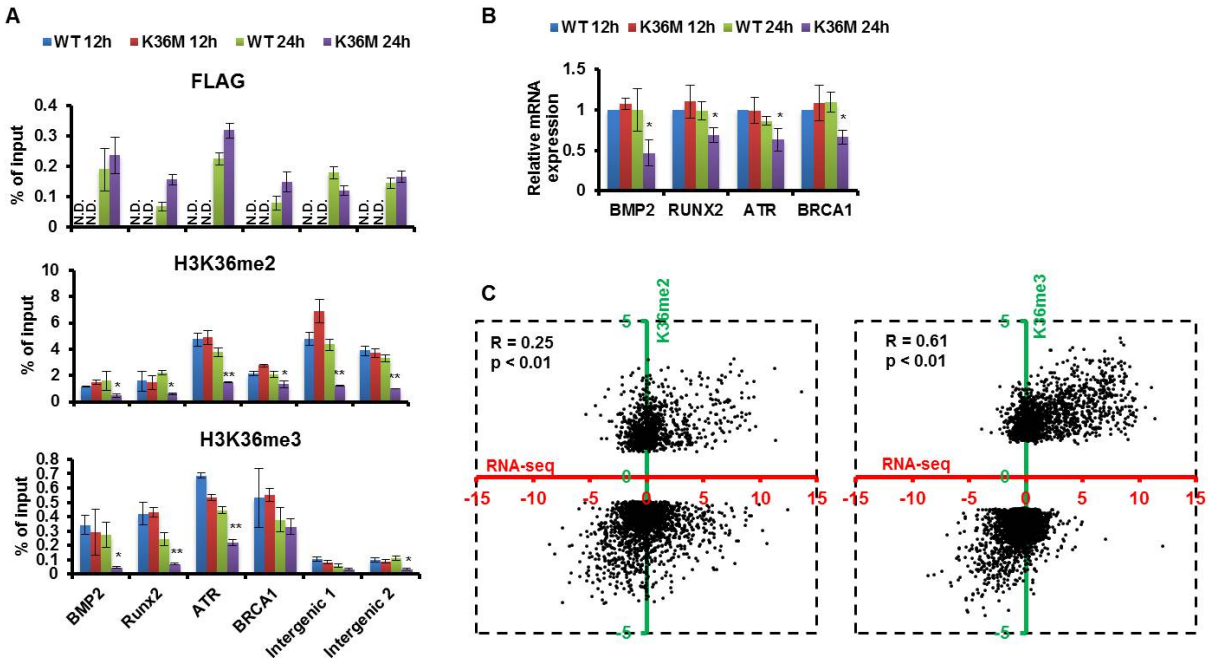

Figure S11. Dynamic relationship between the incorporation of H3.3K36M mutant proteins, changes in H3K36me2/me3 occupancy, and gene expression. (**A**) Incorporation of H3.3K36M mutant protein and reduction of H3K36me2/me3 at different loci occurs with similar kinetics. After transduction of T/C28a2 cells with lenti-viruses carrying FLAG-tagged histone H3.3WT or H3.3K36M for 12 or 24 hours, cells were collected for ChIP assay using antibodies against the FLAG epitope (H3.3 or H3.3K36M, upper panel), H3K36me2 (middle panel) and H3K36me3 (lower panel). Data represents the average and standard deviations of three independent experiments. N.D. Not Detectable (*p<0.05, **p<0.01). (**B**) Expression of *BMP2*, *RUNX2*, *ATR*, and *BRCA1* are reduced 24 hours after transduction of H3.3K36M-expressing lenti-virus. Gene expression was analyzed by real time RT-PCR and was normalized against *ACTB*. mRNA levels detected in cells transduced with H3.3 WT-expression virus for 12 hours were used as references. Results are the mean and standard deviation of three independent experiments (*p<0.05). (**C**) Changes in H3K36me2 (left) and H3K36me3 (right) in chondroblastoma samples correlate with alterations gene expression. The analysis was performed as described in Fig. 4A and genes with significantly changed H3K36me2 or H3K36me3 in two chondroblastoma samples were chosen for analysis.

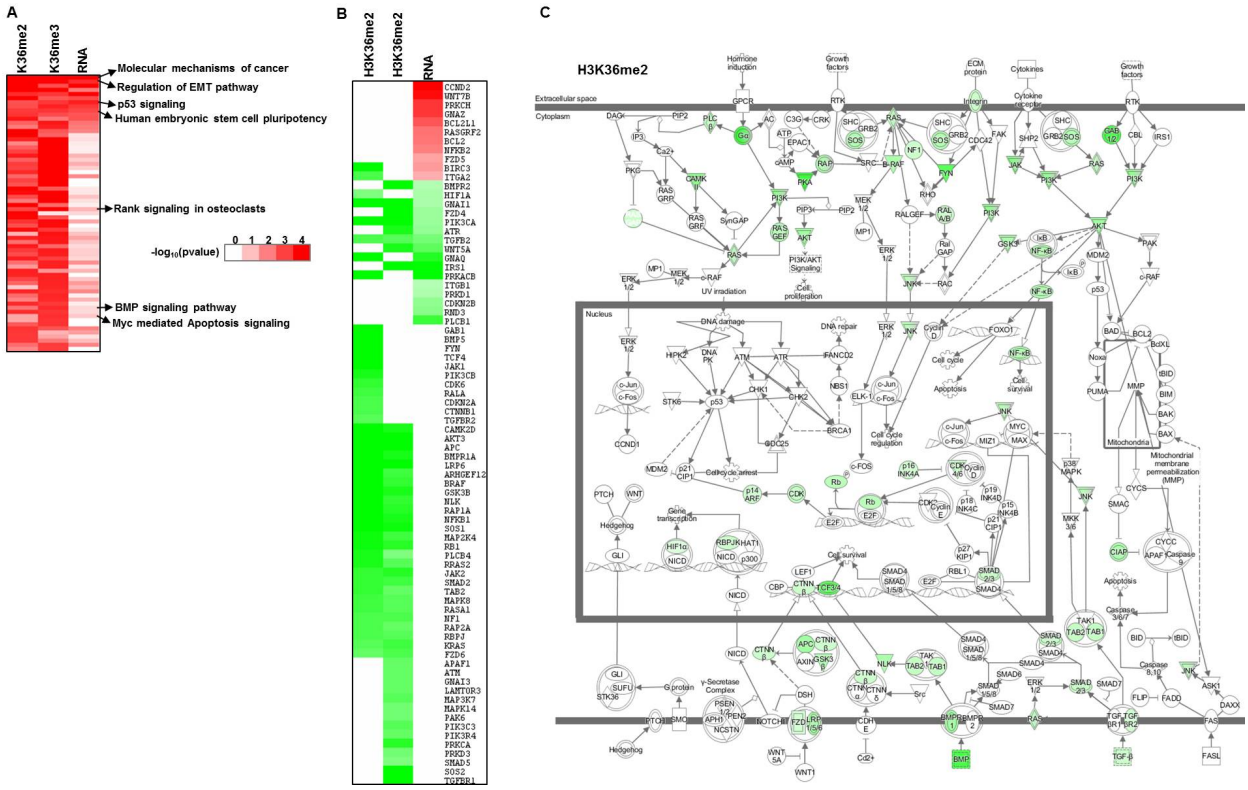

Figure S12. Genes with altered H3K36me2, H3K36me3 and gene expression in two H3.3K36M mutant cell lines and chondroblastoma tissues are enriched in the IPA canonical pathway "Molecular Mechanisms of Cancer". (**A**) The heatmap showing the P values from the pathway analysis of genes with altered H3K36me2/me3 within gene bodies detected by ChIP-seq and transcript expression detected by RNA-Seq. Only genes that are altered in both H3.3K36M cell lines and chondroblastoma tissue samples were chosen for Ingenuity Pathway Analysis (IPA, (http://www.ingenuity.com/). Heatmap shows the -$\log_{10}$ (p) values for the IPA pathways detected in gene sets with altered H3K36me2 (2098 genes) and H3K36me3 occupancy (1013 genes) and gene expression (598 genes) in both H3.3K36M chondrocyte cells and chondroblastoma tumor tissues. P values in this analysis represent the likelihood that the association between each gene set and a given process or pathway is due to random chance. Only the pathways with $p<0.001$ in at least one dataset are shown. Full results were presented in Table S2, and some pathways altered in all three datasets are highlighted in the panel. (**B**) The ratio of H3.3K36M/WT for genes classified in the IPA canonical pathway is shown. Red and green color represents genes with significantly increased and decreased H3K36me2, H3K36me3 occupancy or expression, respectively. (**C**) Genes with altered H3K36me2 occupancy in both H3.3K36M cell lines and chondroblastoma tissues were mapped to the IPA pathway "Molecular Mechanisms of Cancer". Green color represents genes with significantly decreased H3K36me2 occupancy in H3.3K36M. Gray represents genes without changes in H3K36me2.

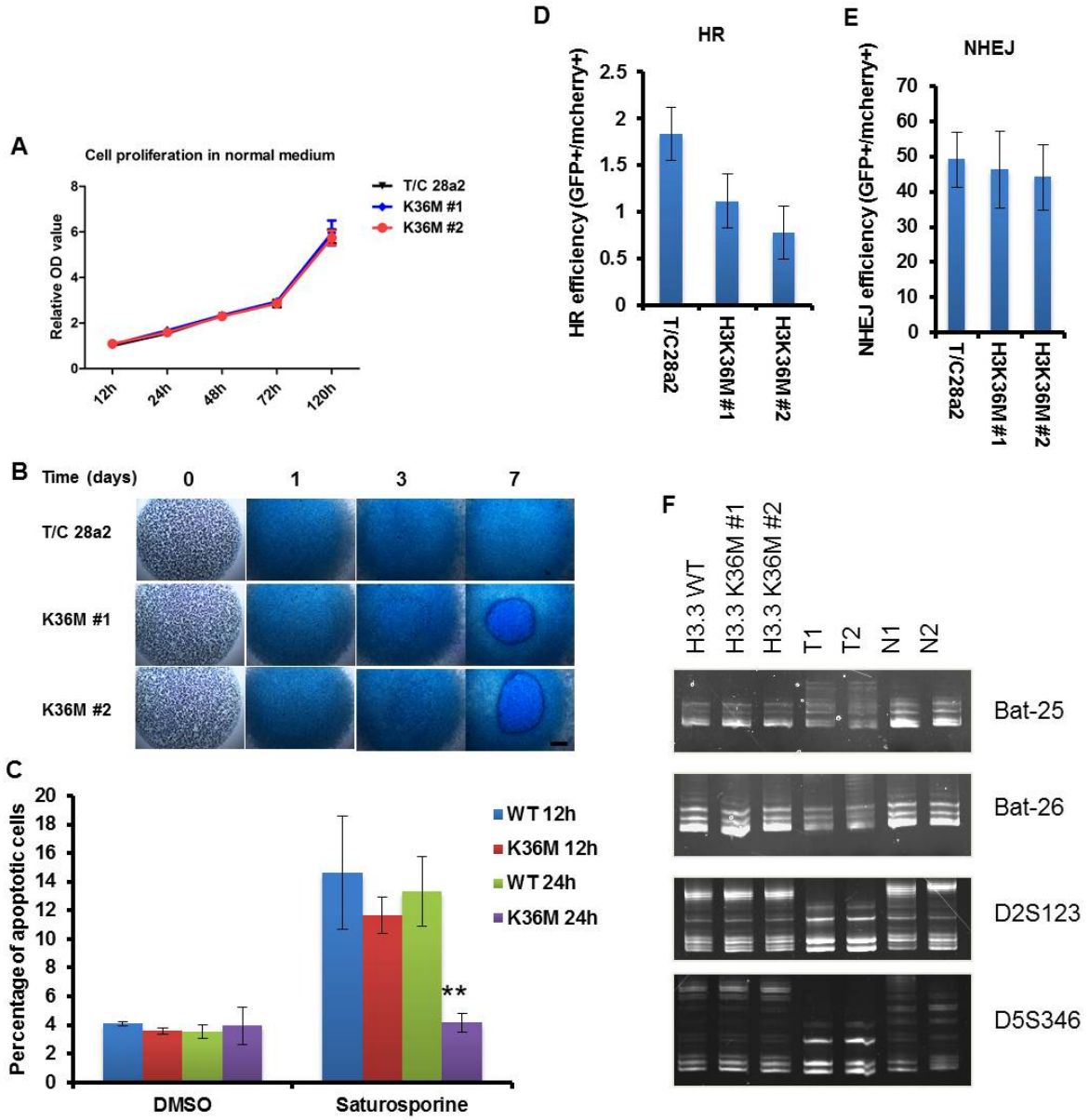

Figure S13. H3.3K36M does not affect chondrocyte proliferation, but improves survival and alters chondrogenic differentiation and DNA repair. (**A**) H3.3K36M has no apparent effect on cell proliferation in normal growth medium. The mean ± SD were shown from three independent experiments. (**B**) H3.3K36M mutant cells show altered chondrogenic differentiation. Images from Alcian blue staining of micromasses differentiated in chondrogenic medium for the indicated number of days are shown here. Scale bar: 50 μm. (**C**) Cells transiently expressing the H3.3K36M mutant proteins are resistant to staurosporine-induced apoptosis. 12 hours or 24 hours after transduction of lentivirus expressing H3.3WT or H3.3K36M, cells were treated with 0.5 μM of staurosporine or DMSO control for three hours and were used for Annexin V/PI staining. The annexin V positive cells were analyzed and quantified by FACS. Data represents the average and standard deviations of three independent experiments (**p<0.01). (**D-E**) Homologous recombination, but not non-homologous end joining was reduced in H3.3K36M T/C28a2 cells. GFP reporter plasmids for homologous recombination (HR) (D) or non-homologous end joining (NHEJ) (E) were co-transfected with the plasmids expressing I-SceA and mCherry. GFP- and mCherry-positive cells were analyzed by flow cytometry 24 hours after transfection. (**F**) H3.3K36M mutation has

no effect on microsatellite instability. Genomic DNA was isolated from parental and two H3.3K36M T/C28a2 cells. Four microsatellite markers were analyzed by PCR. Microsatellite markers were also analyzed in two positive control samples with known microsatellite instability (T1 and T2) and in two negative control samples (N1 and N2).

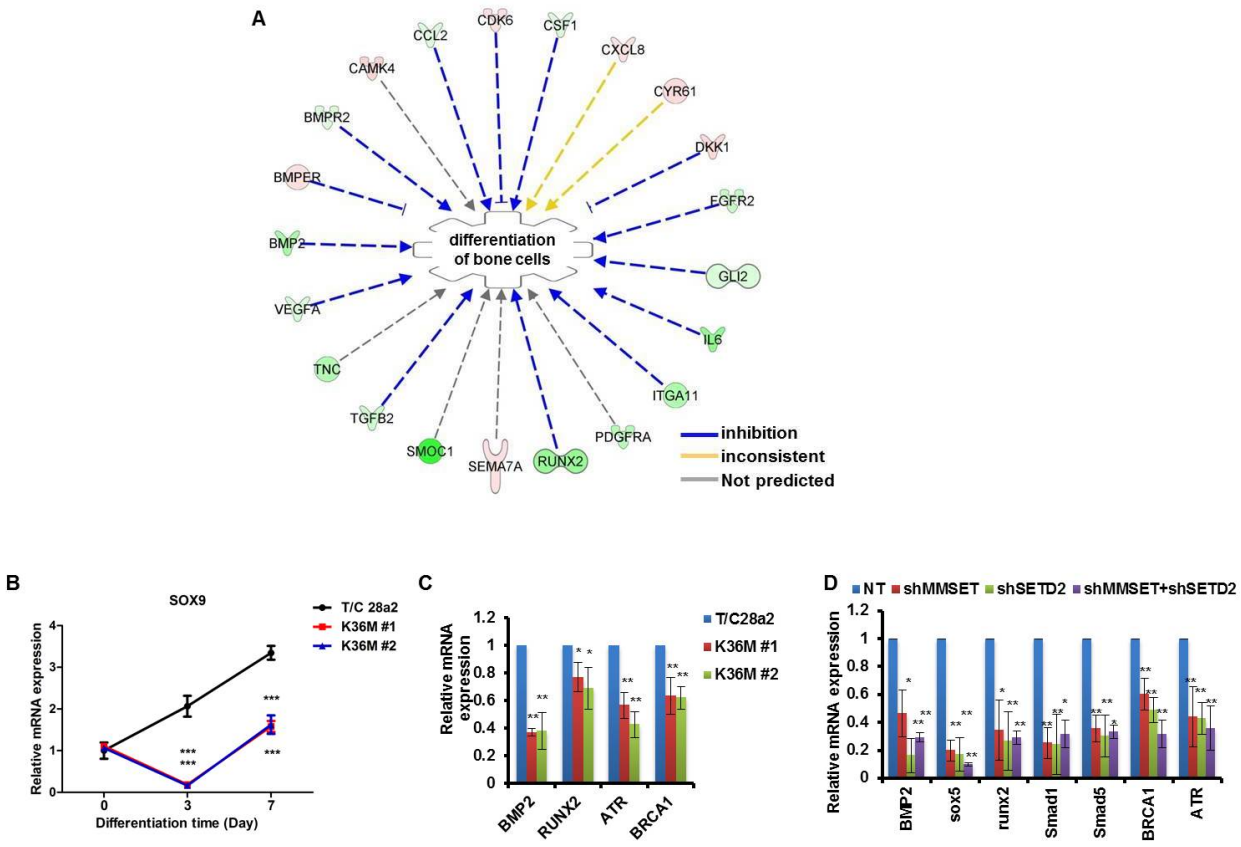

Figure S14. Expression of key genes that regulate differentiation and DNA repair is reduced in H3.3K36M mutant lines and in cells with depletion of *MMSET* and/or *SETD2*. (**A**) Ingenuity Pathway Analysis (IPA) identifies a network of genes whose expression is altered to inhibit the differentiation of bone cells. Nodes represent the genes with altered expression in H3.3K36M chondrocyte cells based on RNA-seq. Red and green color represents up- and down-regulated genes in H3.3K36M cells, respectively. (**B**) Sox9 expression is reduced in H3.3K36M T/C28a2 cells during differentiation. mRNA was isolated from cells during the course of differentiation as described in Fig. 4F and analyzed by RT-PCR (***P<0.001). (**C**) Expression of *BMP2*, *RUNX2*, *ATR*, and *BRCA1* is reduced in H3.3K36M cell lines compared to the parental cell line. The expression of different genes was analyzed by real time RT-PCR and normalized against *ACTB*. The expression level of each gene in parental cells was set to 1. Results (mean and standard deviation, *P<0.05, **P<0.01) from three independent experiments are shown. (**D**) The expression of *BMP2, SOX5*, *RUNX2*, *ATR*, and *BRCA1* is reduced in cells depleted with MMSET, SETD2 alone or in combination. Results are shown as the mean and standard deviation from three independent experiments (*P<0.05, **P<0.01). NT, none-targeted control.

Supplemental Tables

Table S1. Genotype information of patient tumor samples

Diagnosis	No.	Sample ID	*H3F3A*	*H3F3B*	*H3F3B* mutation%*
Chondroblastoma	1	T-03-472	WT	K36M	18%
	2	T-04-481	WT	K36M	25%
	3	mr12-2519	WT	K36M	31%
Giant Cell Tumor	1	T-96-035	G34W	WT	17%
	2	T-99-124	G34W	WT	24%
	3	mr12-5013	G34W	WT	7%

* % cells with mutation in tumor tissues were estimated based on RNA-seq results.

Table S2: A list of genes in Molecular Mechanism of Cancer based on the IPA pathway

Genes with altered H3K36me2, H3K36me3 within gene bodies detected by ChIP-seq and expression detected by RNA-Seq in both H3.3K36M cell lines and chondroblastoma tissue samples were chosen for Ingenuity Pathway Analysis (IPA, http://www.ingenuity.com). The table shows the $-\log_{10}$ (p) values for the IPA pathways detected in gene sets with altered H3K36me2 (2098 genes) and H3K36me3 occupancy (1013 genes) and gene expression (598 genes) in both H3.3K36M chondrocyte cells and chondroblastoma tumor tissues.

Table S3: A list of ChIP-seq and RNA-seq datasets used in this study.

Table S4 Oligonucleotides used in the study.

Name	5'- Sequence -3'	Application
	Genome editing of the H3F3B gene	
gRNA	5'-CACCAGGAAAAGCGCTCCCTCTAC 5'-AAACGTAGAGGGAGCGCTTTTCCT-'3	Targeting on H3F3B
ssDNA	5'- ACCGGTGGGAAAGCCCCCCGCAAACAGCTGG CCACGAAAGCCGCCAGGAAAAGCGCTCCCAGT ACCGGCGGGGTGATGAAGCCTCATCGCTACAG GTAGGTCGGGCGGGGGAACAATGGCCCGGCG GTGGCCGGCTTTGTGCGGCAGCGTCCG-3' (The underline indicates the K36M mutation)	Donor DNA template
Sequencing Primer	F- TCGAGGAAGGGAAGTGACTCCT R- AGAGCCGCACTATTAATCCCA	Amplify H3F3B
	ChIP q-PCR primers	
BMP2	F- CCACTGAGAAGAGTCCAGGTTC R- GGGGAGTATCAGGCCAATAGAG	H3K36me2/me3 ChIP
RUNX 2	F- CTCAGCCAGCCCATCTACAG R- TAACACAGTGGCCTTGGAGG	H3K36me2/me3 ChIP
SOX9	F- TTCTTCTTCCTTAAAGACATTTAAGC R- GGATAGGTCATGTTTGTGTCTTGG	H3K36me2 ChIP
CDK6 1	F- CCCTCAGCTGGAAGACATCC R- CTCCTAGAAGGGGACAAGAAC	Flag/H3K36M ChIP
CDK6 2	F- GCAGGGCTGAAGCCGTCTTC R- GGTAGCGGCGCAACACAATG	Flag/H3K36M ChIP

ACTB	F-CCTCATGGCCTTGTCACAC R-GCCCTTTCTCACTGGTTCTCT	Flag/H3K36M ChIP
Ch19-intergenic	F- AGCTTGTCTTTCCCAAGTTTACTC R- TAGCTGTCGCACTTCAGAGGA	H3K36me3 ChIP
KIAA1432	F- CTCGTTTTTCAGGTCACCGAC R- ACATCTGTCTTTTACAGTTGATGTT	H3K36M ChIP
NSMCE2	F- TCACAATGCCTTCCTGGTTAGT R- TCAAATTTAGGACGCTGTAGGAAG	H3K36M ChIP
Intergenic	F- GTGAGAGGAATCACATTGTGGAGA R- AGTCCTTTTCCCACCTCTAGC	H3K36M ChIP
Intergenic 1	F- GGAACCTCCAGTGCAGTCTTT R- GAAGGGGCTCAGATGCAAGA	H3K36me2/me3 ChIP
Intergenic 2	F- AAATCCATGCCCCTTCCACG R- AGCACATCTCTGGGCAATGA	H3K36me2/me3 ChIP
BRCA1	F- TGCCAGAATGAGAAAGAACATCC R- TGACAATCAGTGATCAGGAAAATCC	H3K36me2/me3 ChIP
ATR	F- ACGGACAGTTGGGAGGTATC R- GCCTAGCGGTTTCTGTGTAGT	H3K36me2/me3 ChIP
	RT-PCR primers	
BMP2	F- TACATGCTAGACCTGTATCGCAG	NM_001200.2

	R-AAAGAAGAATCTCCGGGTTG	
RUNX2	F- ATGTGTTTGTTTCAGCAGCA R- TCCCTAAAGTCACTCGGTATGTGTA	NM_001015051
SOX9	F- TGTATCACTGAGTCATTTGCAGTGT R- AAGGTCTGTCAGTGGGCTGAT	NM_000346.3
ATR	F- GGCCAAAGGCAGTTGTATTGA R- GTGAGTACCCCAAAAATAGCAGG	NM_001184
BRCA1	F- GAAACCGTGCCAAAAGACTTC R- CCAAGGTTAGAGAGTTGGACAC	NM_007297
ACTB	F-AGGCACCAGGGCGTGAT R- CCCACATAGGAATCCTTCTGA	NM_001101.3

_H3F3A_ and _H3F3B_ gene amplification

H3F3A

F-AAA TCG ACC GGT GGT AAA GC

R-ATA CAA GAG AGA CTT TGT CCC A

H3F3B

F-GTA AGT CCA CCG GTG GGA AA

R -AGG AGT GAG CGG ACG CTG CC

Supplemental materials and methods

Cell lines and cell culture: The immortalized human juvenile costal chondrocyte cell line, T/C28a2, was cultured in normal growth medium: DMEM supplemented with 10% fetal bovine serum (FBS) and 1% antibiotic solution as previously described (*10, 24*). To induce differentiation, T/C28a2 cells were cultured in the differentiation medium: DMEM supplemented with 5% FBS, 1% antibiotic solution, 50 μg/ml ascorbic acid, 10 mM β-glycerol-phosphate, and 1X Insulin-Transferrin-Selenium (ITS) (Invitrogen, Carlsbad, CA) as previously described (*25*).

Human primary bone cells were generated from surgical waste of bone tissues collected from the patients undergoing elective orthopedic procedures at Mayo Clinic (Rochester, MN) under IRB approved protocol (IRB# 13-005619). Bone tissues were trypsinized overnight, washed thoroughly with PBS, and minced using a scalpel. The minced tissues were incubated in Advanced MEM supplemented with 10% FBS and 1% antibiotic solution at 37°C and 5% CO_2, and were plated into new culture dishes and passaged 3 times at which time they were used as references/control cells for ChIP-seq and RNA-seq assays of chondroblastoma samples.

HEK293T cells were purchased from ATCC (Manassas, VA). HEK293T cells stably expressing empty vector, FLAG-tagged histone H3.3, or FLAG-tagged histone H3.3 K36M were established by lenti-viral transduction and selection with 1 μg/ml puromycin. They were maintained in the DMEM supplemented with 10% FBS, 1% antibiotic solution, and 1 μg/ml puromycin.

CRISPR/Cas9-mediated genomic knock-in of the *H3F3B* K36M mutation: The gRNAs to target the *H3F3B* gene were identified using the http://crispr.mit.edu/ design tool (Table S4) and were cloned into pSpCas9(BB)-2A-Puro (Addgene, PX459). T/C28a2 cells were co-transfected with the vectors expressing gRNA and Cas9 endonuclease along with donor single-stranded oligonucleotide corresponding to the H*3F3B* WT or *H3F3B* K36M mutation (Table S4) using Nucleofector Kit V (Lonza, Basel, Switzerland) according to the published protocol (*26*). Cells were selected with 1 μg/ml puromycin and individual clones were picked under a microscope. Genomic DNA was isolated from each clone for genotyping using Gentra Puregene kit (Qiagen, Valencia, CA). PCRs were performed using the primers surrounding the target site (Table S4). The resulting PCR products (690 bp) were purified and sequenced to determine the genotype in the *H3F3B* locus. Two independent T/C28a2 clones harboring the *H3F3B* K36M mutation were identified.

Human patient samples: Human chondroblastoma and giant cell tumor samples were collected at Mayo Clinic (Rochester, MN) under the Mayo Clinic IRBe # 13-002254. Table S1 shows mutations of histone H3 genes in patient tumor samples from three chondroblastomas and three giant cell tumors of bone. The genotype of tumor samples was determined by Sanger sequencing of PCR amplicons of *H3F3A* and *H3F3B* genes and was validated by RNA-seq. The percentage of mutant transcript was determined by read counts of RNA-seq. All collected tissues were stored at −80°C until analyzed.

Preparation of tissue or cell extracts and Western blotting analysis: For acid extraction of core histones, tissue (~30 mg) were homogenized and incubated in 400 μl 0.4N HCl solution for 30 min at 4°C. Extracted histones were precipitated with trichloroacetic acid (TCA), washed with ice-cold acetone twice and dissolved in 1X SDS sample buffer. Similar procedures were also followed to extract histone from cell lines for Western blot or mass spectrometry analysis described below (*27*). Whole cell extracts were prepared by re-suspending cells with 1X SDS sample buffer.

For Western blotting analysis, antibodies against H3K36me2 (Cell Signaling Technology, Cat.# 2901, lot 5), H3K36me3 (Active Motif, cat. # 61101, lot 32412003), H3K27me3 (Cat.#9733), EZH2 (Cat.#5246), SUZ12 (Cat.#3737) and Ring1B (Cat.#5694) were purchased. The antibody (Cat.# 31-1085-00) recognizing H3K36M mutant proteins was obtained from RevMAb Biosciences. Antibodies against

H3K4me3 (Cat.#07-473), NSD1 (Cat.#04-1565), ASH1L (Cat.#ABE204), and MMSET (Cat.#ab75359) were purchased from Millipore. NSD2 (Cat.# ab75359) and EGFP (Cat.#ab6556) antibodies were obtained from Abcam. Antibodies against α-Tubulin (Cat.#T9026) and FLAG epitope (Cat.#F1804) were purchased from Sigma. Antibodies against H3K9me3, Histone H4, H4K20me2, H4K20me3, and histone H3 were previously described (*28, 29*). Quantification of Western blot analysis was performed by ImageJ, and relative intensity towards the control was reported at the bottom of each Western blot.

Chromatin immunoprecipitation-deep sequencing (ChIP-seq) and ChIP-qPCR: Frozen tissues were cut, divided into 50 mg aliquots, and stored in tubes at -80°C. The frozen tissues were homogenized on ice for 15–30 seconds in 500 μL 1X PBS using a tissue grinder (ACTGene, Piscataway, NJ). Tissue homogenates or cultured cells were cross-linked with 1% formaldehyde (final concentration) for 10 min and quenched with 125 mM glycine for 5 min at room temperature and washed once with TBS. The pellets were resuspended in cell lysis buffer (10 mM Tris-HCl, pH7.5, 10 mM NaCl, 0.5% NP-40) and incubated on ice for 10 min. Lysates were divided into two aliquots and washed with MNase digestion buffer (20 mM Tris-HCl, pH7.5, 15 mM NaCl, 60 mM KCl, 1 mM $CaCl_2$). After re-suspending in 500 μL MNase digestion buffer containing a proteinase inhibitor cocktail (Sigma, St. Louis, MO), the lysates were incubated in the presence of 1,000 units of MNase (NEB, Ipswich, MA, Cat.# M0247S) at 37 °C for 20 min with continuous mixing in thermal mixer (Fisher Scientific, Pittsburgh, PA). After adding the same volume of sonication buffer (100 mM Tris-HCl, pH8.1, 20 mM EDTA, 200 mM NaCl, 2% Triton X-100, 0.2% sodium deoxycholate), the lysates were sonicated for 15 min (30 sec on / 30 sec off) using Bioruptor Twin (UCD-400) (Diagenode, Inc., Denville, NJ) and centrifuged at 21,130 x g for 10 min. The supernants were collected and the chromatin content was estimated by the Qubit assay (Invitrogen). For the normalization of ChIP efficiency, yeast chromatins equivalent to about 0.5 % of total input chromatin of control and each target sample was added. The chromatin was then incubated with 2 μg of rabbit polyclonal anti-H3K36me3 antibody (Active Motif, Carlsbad, CA, Cat.# 61101, lot # 32412003), 1.5 μg of rabbit monoclonal anti-H3K36me2 antibody (Cell Signaling Technology, Danvers, MA, Cat.#2901, lot# 5), or 2 μg of rabbit monoclonal anti-H3K36M antibody (RevMAb Biosciences, Cat.# 31-1085-00, lot# O-08-00294) on a rocker overnight. Protein G-magnetic beads (30 μL, Life Technologies, Carlsbad, CA) were added for 3 hour incubation. The beads were extensively washed with ChIP buffer (50 mM Tris-HCl, pH8.1, 10 mM EDTA, 100 mM NaCl, 1% Triton X-100, 0.1% sodium deoxycholate), high salt buffer (50 mM Tris-HCl, pH8.1, 10 mM EDTA, 500 mM NaCl, 1% Triton X-100, 0.1% sodium deoxycholate), LiCl buffer (10 mM Tris-HCl, pH8.0, 0.25 M $LiCl_2$, 0.5% NP-40, 0.5% sodium deoxycholate, 1 mM EDTA), and TE buffer. Bound chromatin was eluted and reverse-crosslinked at 65°C overnight. DNAs were purified using Min-Elute PCR purification kit (Qiagen, Valencia, CA) after the treatment of RNase A and proteinase K. ChIP enrichment was validated by performing real-time PCR in the genomic loci targeting the gene body and the neighboring intergenic region of *ACTB* gene (Table S4). ChIP-seq libraries were prepared from 10 ng ChIP and input DNA using the Ovation ultralow DR Multiplex kit (NuGEN, San Carlos, CA). The ChIP-seq libraries were sequenced to 51 base pairs from both ends on an Illumina HiSeq 2000 instrument in the Mayo Clinic Center for Individualized Medicine Medical Genomics Facility. ChIP-qPCR was assessed on indicated genomic regions using SYBR Green Supermix (Bio-Rad Laboratories, Hercules, CA). Table S4 shows the primer information used in the study. The comparative ΔCt method was used to determine relative enrichment compared with input.

H3K36M ChIP-seq data analysis: Paired-end reads from H3.3K36M ChIP-seq were aligned to the human genome (hg19) using the Bowtie2 (*30*) software. Consistent pair reads were used for further analysis. Genome-wide read coverage was calculated by BEDTools (*31*) and in-house Perl programs. The read density scan was performed by in-house Perl programs using the traditional normalization method: Reads Per Kilobase per Million mapped reads (RPKM). The H3.3K36M peaks were identified using MACS2 (*32*) using 0.001 as the cutoff p value.

Normalization of H3K36me2 and H3K36me3 ChIP-seq with spiked-in yeast chromatins: H3K36me2 and H3K36me3 ChIP-seq sequence reads were mapped and normalized according to published procedures (*33*). Human (hg19) and yeast (saccer3) genomic sequences were combined. Bowtie2-build code was used to build a custom Bowtie2 library for the combined genome sequence. All sequence reads from spike-in ChIP-seq experiment were aligned against the custom library using Bowtie2 default parameters. The consistent pair reads were separated into each organism. The H3K36me2 and H3K36me3 ChIP-seq peaks were identified by MACS2 using the broad peak calling parameter; and the p value of cutoff is set to 0.001. To identify the genes showing differential occupancy of H3K36me2 and H3K36me3 marks between *H3F3B* WT or *H3F3B* K36M mutant cells or tissues, the number of reads in gene body was counted by BEDTools and normalized by the factor determined by sequences reads of yeast chromatin. P value was calculated using DESeq (*34*) with 10^{-5} as the cutoff p value.

Histone extraction and Derivatization: Histones were extracted as previously described (*27*). Histone proteins were chemically acetylated with ($^{13}C_2$, d_3)-acetyl N-hydroxysuccinimide ester to block unmodified and monomethylated lysines (delta mass +47.036094 Da) and then digested by trypsin as previously described (*35*). The peptides were desalted with C18 Stagetip (3M Corporation, St. Paul, MN) (*36*) prior to LCMS analysis.

LC-MS/MS: The tryptic peptides were analyzed by nano-flow liquid chromatography electrospray tandem mass spectrometry (nanoLC-ESI-MS/MS) using a Thermo Scientific Q-Exactive-Plus Mass Spectrometer (Thermo Fisher Scientific, Bremen, Germany) coupled to a Thermo Ultimate 3000 RSLCnano HPLC system. The peptide mixture was loaded onto a 250nl OPTI-PAK trap (Optimize Technologies, Oregon City, OR) custom packed with Michrom Magic C18 5um solid phase (Michrom Bioresources, Auburn, CA). Chromatography was performed using 0.2 % formic acid in both the A solvent (98%water/2%acetonitrile) and B solvent (80% acetonitrile/10% isopropanol/10% water), and a 5%B to 15%B gradient over 26 minutes, then 15%B to 35%B over 16 minutes at 300 nl/min through a hand packed 75μm x 330mm PicoFrit column with Agilent Poroshell 120 EC C18 stationary phase. The Q-Exactive-Plus mass spectrometer was set up with a FT survey scan from 300-1600 m/z at resolution 70,000 (at 200m/z), followed by HCD MS/MS scans on the top 12 ions at resolution 17,500 with the normalized collision energy (NCE) setting at 28. The MS1 AGC target was set to 1e6 and the MS2 target was set to 1e5 with max ion inject times of 50ms for both. The targeted MS/MS data acquisition was achieved with the inclusion list function with no dynamic exclusion. The inclusion list was built based on human histone H3 K27-R40 peptide sequences for both histone H3.1 and H3.3 variants. For each peptide, isoforms with 5 possible modification groups on 3 lysine residues (K27, K36 and K37) at all charge states were considered – mono-, di-, tri-methylation, acetylation and unmodified have delta mass of 61.051744 (methyl group + heavy acetyl group), 28.0313, 42.04695, 42.010565 and 47.036094 Da, respectively.

Peptide identification and quantitative analysis: Data were searched against the Uniprot Homo sapiens proteome database (http://www.uniprot.org) using Morpheus search engine (http://morpheus-ms.sourceforge.net/) as previously described which is optimized for analyzing MS data containing high resolution MS2 spectra (*37*). Five modifications on lysine and methionine oxidation were chosen as variable modifications, with 6 ppm as the precursor mass error and 0.025 Da as fragment mass error. All peptide-spectra matches were filtered at 1% False Discovery Rate and 1% Q-value. The peptide identifications were manually evaluated in a stringent manner to eliminate false positive identifications and correctly assign the modification sites. HPLC chromatogram analysis confirmed good separation of modification isoforms. Relative levels of each K36 modification were calculated based on the intensities of precursor ions using in-house developed scripts following previously described strategies (*38, 39*). Briefly, the relative modification level was calculated as the percentage of the total precursor ion intensities comparing between the peptides carrying a specific modification (e.g. K36 trimethylation) and the peptides of all isoforms containing the residue (e.g. K36). Statistical significance analysis was conducted with student's t-test using SAS statistical software 9.3 (SAS Institute Inc., Cary, NC).

Reverse transcription (RT)-PCR: Total RNA was extracted using the miRNeasy Mini kit (Qiagen, Valencia, CA). cDNAs were synthesized from 0.5 μg of total RNA using random hexamers (Invitrogen, Carlsbad, CA). Real-time PCRs were performed in 25 μL reactions containing 0.1 μM primers and SYBR Green PCR Master Mix (Bio-Rad Laboratories, Hercules, CA). β-actin was used as a control to normalize the expression of target genes. Table S4 shows primer sequences for RT-qPCR.

RNA-seq: RNA-seq libraries were prepared with ovation RNA-seq system v2 kit (NuGEN) according to the manufacturer's instruction, and were sequenced on an Illumina HiSeq 2000 instrument in the Mayo Clinic Center for Individualized Medicine Medical Genomics Facility. Sequence reads from RNA-seq samples were aligned to the human genome hg19 and gene annotations from Refseq gene using TopHat v2.05 (*40*). Cufflinks v2.0.2 was used to calculate FPKM values of genes (*41*). Differential gene expression was analyzed by Cuffdiff using cutoff FDR (false discovery rate) < 0.05 (*41*).

***In vitro* histone methyltransferase assay:** The catalytic SET domain (amino acid 941-1365) of human MMSET was cloned into pGEX-6p-1 vector. The full-length cDNA of human MMSET was a kind gift from Dr. Zhenkun Lou (Mayo Clinic, Rochester, MN). The expression vectors encoding human SETD2 catalytic domain (pET28a-MHL hSET2 1433-1711), human ASH1L catalytic domain (pET28a-smt3 hASH1 2074-2293), or human NSD1 catalytic domain (pGEX-6p-1 hNSD1 1849-2094) were previously described (*42-44*). The proteins were purified following published protocols (*13, 42*). Histone methyltransferase assays were performed using reconstituted H3.3 nucleosomes and purified catalytic domain of each methyltransferase in the presence of different amounts of histone H3.3 K36 WT peptide (PSTGGVKKPHRYRC) or histone H3.3K36M peptide (PSTGGVMKPHRYRC). Mononucleosomes containing wild type H3.3 or H3.3K36M mutants were reconstituted as described (*45, 46*). The reactions were carried out for 1 h at 30 °C in a 25 μl reaction mixture containing 1 μg of wild type nucleosomes or a fraction of H3.3K36M mononucleosomes (0.5 or 0.25 μg), a purified protein (0.2 μg MMSET, 1 μg SETD2, 0.8 μg ASH1L, or 1.3 μg NSD1), 1 μl of S-adenosyl-[methyl-^{3}H]-l-methionine, 50–85 Ci/mmol, 0.55 mCi/ml (Perkin Elmer Life Sciences), histone H3 peptide (or H3 K36M peptide). The reactions were stopped by the addition of SDS sample buffer and were separated by 13% SDS-PAGE. The gel was stained with Coomassie Brilliant Blue, sprayed with ^{3}H-ENHANCE (PerkinElmer Life Sciences), and analyzed by fluorography. For the scintillation count, the samples were spotted on P81 paper, washed with sodium phosphate buffer (pH 9.0), and quantitated by liquid scintillation counter.

Mononucleosome immunoprecipitation and peptide pull-down assays: Mononucleosome immunoprecipitation (IP) was performed in HEK293T cells stably expressing FLAG-tagged histone H3.3 or FLAG-tagged histone H3.3 K36M proteins. Cells were fixed with 1% formaldehyde for 3 min, quenched with 125 mM glycine for 5 min at RT, and lysed with lysis buffer (10 mM Tris-HCl, pH7.5, 10 mM NaCl, 0.5% NP-40) on ice. Chromatin extracts from 7 X 10^{8} cells were digested with 7 X 10^{5} U MNase (NEB, Cat. # M0247S) at 37°C for 20 min. The nucleosomes were extracted in IP buffer (50 mM Tris-HCl, pH8, 10 mM EDTA, 100 mM NaCl, 1% Triton X-100, 0.1% sodium deoxycholate). Nucleosomes were incubated with 30 μl of prewashed anti-FLAG M2 agarose beads (Sigma) at 4°C overnight. The beads were extensively washed with wash buffer (50 mM HEPES-KOH, pH 7.4, 200 mM NaCl, 0.5% Triton X-100, 10% glycerol, 10 mM EDTA). Proteins were eluted by 1 mg/ml FLAG peptide at 16°C for 30 min, precipitated by TCA, and analyzed by Western blotting.

Histone H3.3K36 peptide, H3.3 K36M peptide, and H3 K9WT peptide (peptide sequence: TARKSTGC) were conjugated into SulfoLink agarose beads according to the manufacturer's instructions. Peptide-conjugated beads were incubated with nuclear extracts at 4°C for 3 h. The beads were washed with washing buffer D (20 mM HEPES, pH 7.9, 20% glycerol, 0.2 mM EDTA, 0.2% Triton X-100, and protease inhibitors) containing 100 mM, 200 mM, or 400 mM NaCl to measure the binding affinity of each methyltransferase with peptides. Remaining proteins on beads were eluted by SDS sample buffer and analyzed by Western blotting.

Cell proliferation, colony formation, and differentiation assays: 1.5×10^3 T/C28a2 cells were plated in each well of 96-well plate with 200 μl of normal growth medium. After 12 h, the medium was changed with either normal growth medium or differentiation medium. Cells were counted every 24 h by the cell titer blue assay kit (Promega, Madison, WI, Cat # G8081) according to the manufacturer's instructions.

For colony formation assays, 400 cells were seeded to each well of 6 well plates. Then the cells were cultured for 3 weeks before crystal violet staining.

For differentiation of T/C28a2 cells, a 10 μl drop of normal growth medium containing 2×10^5 cells was placed into micromass in 60 mm dishes as previously described (*47*). After 5 hours, 3 ml differentiation medium was added to the wells. Fresh differentiation medium was added to the dishes every 3 days during the 3-week culture period. Aggregate culture in the basal medium alone without supplemental factors was used as the negative control. Micromasses were fixed at indicated time points with 10% neutral buffered formalin for 10 min and then stained with Alcian blue (1% Alcian blue, 3% acetic acid, Sigma, St Louis, MO) for 2 h to detect glycosaminoglycans in the extracellular matrix. The cells were photographed under a microscope (4X objective, Nikon) after several washes with double distilled water.

Annexin V Apoptosis assay: For annexin V apoptosis assay, cells were treated with different concentrations of Staurosporine for 3 hours, and stained with the Alexa Fluor® 488 Annexin V/Dead Cell Apoptosis Kit (ThermoFisher, #V13241) according to the manufacturer's instructions and then analyzed by a mass spectrometry.

Assays for non-homologous end joining (NHEJ) and Homologous-recombination (HR) efficiency: NHEJ assays were performed as described previously (*48*). Briefly, parental or H3.3K36M T/C28a2 cells were co-transfected with pmCherry and linearized Pem1-EGFP-Ad2. pmCherry was used to normalize transfection efficiency. Cells were collected for FACS analysis and GFP-positive cells were counted to determine the NHEJ efficiency. HR assays were performed following published procedures with modification (*49*). Briefly, cells were co-transfected with DR-GFP, I-SceI (pCBA-I-SceI) endonuclease, and pmCherry. The endonuclease was used to induce double-strand breaks and pmCherry was used to normalize transfection efficiency. Cells were harvested 1 day after I-SceI transfection and subjected to flow cytometric analysis. The ratio between GFP- and mcherry-positive cells was used to determine NHEJ and HR efficiency.

Immunofluoresence: Immunofluorescence was performed as previously described (*28, 29*). Cells grown on chamber slides (Nunc) or coverslips were washed briefly with PBS followed by fixation with 3% paraformaldehyde at room temperature for 15 min. Cells were permeabilized with 0.5% Triton X-100 solution for 5 min at room temperature and then blocked with 5% normal goat serum for 1 hour. Primary antibodies with appropriate dilutions (H3K36me3 (1:1000), H3K36me2 (1:2000), H3K36M (1:500)) were added and incubated at 4^oC overnight. Cells were then washed with PBST 3 times and probed with Alexa fluor 488 or 594-conjugated secondary antibodies at room temperature for 1 hour. Cells were then washed 3 times with PBST and DNA was counterstained with DAPI. Samples were mounted with ProLong Gold Antifade reagents (Invitrogen) and examined using a Zeiss Axioplan Fluorescence microscope or Zeiss LSM 780 Confocal Microscope.

Statistical analysis: The p values for the Venn diagrams shown in Fig. 2B, Fig. 3A and Fig. S6A-B were calculated by the hypergeometric test. The p values in Fig. 2D, Fig. 2G, Fig. 3E, Fig. 4B-F, Fig. S3A, Fig. S5E, Fig. S6F, Fig. S9A, Fig. S10B, Fig. S11A-B, Fig. S13C, Fig. S14B-D, were calculated by two-tailed Student's t test. The Chi-square test was used to calculate the p value for the distribution of H3K36me2 peaks (Fig. 2C) and H3K36M peaks (Fig. 3B) among promoters, gene bodies, TES ±2Kbp, and intergenic regions.

Supplemental References:

22. S. Anders, W. Huber, *Genome biology* **11**, R106 (2010).
23. A. Subramanian *et al.*, *Proceedings of the National Academy of Sciences of the United States of America* **102**, 15545-15550 (2005).
24. F. Finger *et al.*, *Arthritis Rheum* **48**, 3395-3403 (2003).
25. E. W. Bradley, M. H. Drissi, *Mol Endocrinol* **24**, 1581-1593 (2010).
26. F. A. Ran *et al.*, *Nat Protoc* **8**, 2281-2308 (2013).
27. D. Shechter, H. L. Dormann, C. D. Allis, S. B. Hake, *Nat Protoc* **2**, 1445-1457 (2007).
28. K. M. Chan *et al.*, *Genes Dev* **27**, 985-990 (2013).
29. K. M. Chan, H. Zhang, L. Malureanu, J. van Deursen, Z. Zhang, *Proc Natl Acad Sci U S A* **108**, 16699-16704 (2011).
30. B. Langmead, S. L. Salzberg, *Nature methods* **9**, 357-359 (2012).
31. A. R. Quinlan, I. M. Hall, *Bioinformatics* **26**, 841-842 (2010).
32. Y. Zhang *et al.*, *Genome biology* **9**, R137 (2008).
33. D. A. Orlando *et al.*, *Cell reports* **9**, 1163-1170 (2014).
34. M. I. Love, W. Huber, S. Anders, *Genome biology* **15**, 550 (2014).
35. T. Zhou, Y.-h. Chung, Y. Chen, (Submitted).
36. J. Rappsilber, M. Mann, Y. Ishihama, *Nat Protoc* **2**, 1896-1906 (2007).
37. C. D. Wenger, J. J. Coon, *J Proteome Res* **12**, 1377-1386 (2013).
38. G. Leroy *et al.*, *Epigenetics Chromatin* **6**, 20 (2013).
39. Y. Zheng, P. M. Thomas, N. L. Kelleher, *Nat Commun* **4**, 2203 (2013).
40. C. Trapnell, L. Pachter, S. L. Salzberg, *Bioinformatics* **25**, 1105-1111 (2009).
41. C. Trapnell *et al.*, *Nat Biotechnol* **28**, 511-515 (2010).
42. Q. Qiao *et al.*, *J Biol Chem* **286**, 8361-8368 (2011).
43. W. Zheng *et al.*, *J Am Chem Soc* **134**, 18004-18014 (2012).
44. S. An, K. J. Yeo, Y. H. Jeon, J. J. Song, *J Biol Chem* **286**, 8369-8374 (2011).
45. P. N. Dyer *et al.*, *Methods Enzymol* **375**, 23-44 (2004).
46. F. Ferron, C. Bussetta, H. Dutartre, B. Canard, *BMC Bioinformatics* **6**, 255 (2005).
47. E. W. Bradley, L. R. Carpio, J. J. Westendorf, *J Biol Chem* **288**, 9572-9582 (2013).
48. A. G. Patel, J. N. Sarkaria, S. H. Kaufmann, *Proc Natl Acad Sci U S A* **108**, 3406-3411 (2011).
49. K. Luo, H. Zhang, L. Wang, J. Yuan, Z. Lou, *EMBO J* **31**, 3008-3019 (2012).